Chapter

Sulfided NiMo/*Clinoptilolite* Catalysts for Selective Sulfur Removal from Naphtha Stream without Olefin Hydrogenation

Cristina Farías Rosales, Rut Guil-López, Marisol Faraldos, Rafael Maya Yescas, Trino Armando Zepeda, Barbara Pawelec and Rafael Huirache-Acuña

Abstract

The natural *clinoptilolite* zeolite has been modified by acid leaching with HNO_3 in order to obtain economic material for supporting NiMoS hydrotreating catalysts. The most optimized zeolite material was obtained by leaching with HNO_3 at 80°C during 24 h. The bimetallic NiMo catalysts prepared by wet impregnation of a zeolite support, followed by calcination and sulfidation, were characterized by several physico-chemical techniques and tested in the hydrodesulfurization (HDS) of 3-methyl-thiophene (3-MT) model feed at atmospheric H_2 pressure and T = 280°C. For all catalysts, the 3-MT transformation mainly occurs via direct desulfurization reaction route being diminished the catalyst hydrogenation function. This was linked with the formation of highly stacked layers of MoS_2 particles having a low amount of "brim sites," as demonstrated by HRTEM. The cause of the best performance of Ni-$Mo_{(H)}$/Z-1 sulfide catalyst in the HDS of 3-MT can be the presence of K^+ impurities on the support surface which forces the formation of highly stacked layers of MoS_2 particles.

Keywords: hydrodesulfurization, acid leaching, *clinoptilolite*, zeolite, naphta

1. Introduction

The use of suitable natural zeolites for supporting heterogeneous catalysts is economically attractive option in many countries possessing abundance of natural zeolites [1]. Among these zeolites, the *clinoptilolite* is of considerable interest due to its effective high cation exchange capacity, unique crystal and pore structure, chemical stability in corrosive media, and thermostability [2]. *Clinoptilolite* has a cage-like structure consisting of SiO_4 and AlO_4 tetrahedral units joined by oxygen atoms. The native charges of the AlO_4 units are balanced by Mg, Ca, Na, K, and/or Fe cations. Moreover, its textural and acid properties should be improved by elimination of the extraframework cations, for example, by chemical leaching [3–5].

Clinoptilolite is crystalline aluminosilicate mineral which exhibits large number of acid sites distributed through the network of channels and cavities

consisting of AlO_4 and SiO_2 tetrahedral units joined by shared oxygen atom [3]. It is a sheet-like structural organization that contains open 10-membered rings (7.5 Å × 3.1 Å) alternated with eight-membered rings (4.6 Å × 3.6 Å, 4.7 Å × 2.8 Å). Those rings are stacking together from sheet to sheet to form channels throughout the crystal structure [3]. The AlO_4 units exhibit negative charge which is compensated by the presence of undesired cations, such as Mg^{2+}, Ca^{2+}, Na^{+}, K^{+}, and/or Fe^{3+}. The number of acid sites and their strength can be controlled by zeolite dealumination, isomorphous substitution of atoms with tetrahedral or via ion exchange methods. The hydroxyl group generation (formation of Brønsted acid sites) can be achieved also by hydrolysis of a zeolite possessing multivalent cations, or by decomposition of the NH_4^{+} ions into the zeolite. In this sense, the study by Arcoya et al. [4] demonstrated that the chemical treatment with NH_4Cl or HCl solutions opened the channels and increased acidity and thermal stability of *clinoptilolite*. On the contrary to HCl treatment, it was reported that HNO_3-treatment led to morphology changes of the raw *clinoptilolite* from the lead-like to the needle-like, an increase of specific surface area and decrease of crystallinity [5].

Recently, there is growing interest in the use of natural zeolites such as *clinoptilolite* as adsorbents [6–11], catalysts [12–17] or for supporting heterogeneous catalysts [18–20]. In particular, the use of modified *clinoptilolite* as catalysts for different catalytic reactions was extensively studied [13–23]. For example, the advantage of base-exchanged natural *clinoptilolite* catalyst for the Knoevenagel reaction was reported [16]. This zeolite demonstrated to be also an effective catalyst for skeletal isomerization of n-butenes to isobutenes [14]. The original *clinoptilolite* zeolite exhibited very low activity in *o*-xylene isomerization, due to limitation by the access of the reactant inside the zeolite channels [4]. However, the zeolite leaching with HCl led to effective catalyst for this reaction [4]. Similarly, the *clinoptilolite* treated with HCl solutions exhibited a good performance in the liquid phase isomerization of α-pinene [12]. In contrast to the HCl treatment, the *clinoptilolite* zeolite treated with NH_4Cl exhibited a low activity in the *o*-xylene isomerization [4]. This was linked with the collapse of part of the zeolite framework producing an increase in the secondary porosity, which enabled the *o*-xylene to reach acid sites [4].

Contrary to the investigation of *clinoptilolite* zeolite as catalyst, its use for supporting hydrotreating catalysts was scarcely studied [4, 18, 23]. In this sense, our previous study on the effect of the incorporation of metals (NiMoW) into this natural Mexican *clinoptilolite* zeolite, followed by sulfidation, demonstrated that those catalysts exhibited low HDS activity, which was explained as due to the low specific area (S_{BET}) of pristine zeolite [23]. It was concluded that the elimination of impurities from the pristine zeolite is needed to increase the zeolite specific surface area. Thus, the aim of present work was to remove those cations from the zeolite structure to enhance the support morphology and textural properties needed for easy reactant and products diffusion into zeolite inner structure. With this objective, acid zeolite leaching at different conditions was employed. The objectives of this acid leaching were various: (i) an increase of the zeolite specific area by chemical leaching of polyvalent cations; (ii) an increase of the catalyst stability by an increase in Si/Al ratio (due to dealumination); (iii) an increase of the catalyst acidity; (iv) the modification of the pore system by incorporation of the metal oxides into internal zeolite porous structure. The effects of zeolite acid leaching and Mo loading on the catalyst behavior of sulfided NiMo/*Clinoptilolite* catalysts were evaluated in the selective hydrodesulfurization (HDS) of 3-methylthiophene (3-MeT) reaction.

2. Experimental

2.1 Modification of the original *Clinoptilolite* by acid treatment

The natural zeolite used for supporting NiMo catalysts was a natural *clinoptilolite* zeolite from the Cuitzeo area deposit (Michoacán, Mexico). For more details on the physicochemical features of this natural mineral, the reader is addressed to Ostrooumov et al. and Huirache-Acuña et al. [3, 23]. Prior to acid leaching, the *clinoptilolite* zeolite was crushed and sieved to obtain particle size <297 mesh. Then, the zeolite was washed with deionized water and dried at 80°C overnight. Element composition of the natural zeolite was investigated by Huirache-Acuña et al. [23].

The acid leaching with 1 M nitric acid (with a proportion of 10 mL of solution per gram of zeolite) was performed at 80°C under stirring for either 24or 48 h. Those zeolite materials will be denoted hereafter as Z-1 and Z-2, respectively. After filtering, the solid was washed repeatedly with excess of distilled water until all traces of nitric acid were removed. Then, the solids were dried at 110°C for 14 h and calcined at static air conditions at 500°C for 5 h.

2.2 Preparation of bimetallic $NiMo_{(x)}$/*Clinoptilolite* catalysts

All oxide catalyst precursors were prepared by co-impregnation taking into account the isoelectric points (PIZ) of Z-1 and Z-2 supports. The measurements of isoelectric points of the *clinoptilolite* zeolite confirmed that zeolite leaching with HNO_3 during different times (24 and 48 h) led to very small change of the isoelectric point (**Figure 1**). An aqueous solutions of ammonium molybdate tetrahydrate ($H_{24}Mo_7N_6O_{24}.4H_2O$) and nickel acetate tetrahydrate ($C_4H_6NiO_4{\cdot}H_2O$) were used as molybdenum and nickel precursors, respectively. The corresponding amount of the metal salts of Mo and Ni were dissolved separately at room temperature in 5 mL of deionized water taking into account the isoelectric point of each zeolite. After impregnation, the catalysts were dried overnight in air at 110°C and then calcined at 500°C for 3 h. The catalysts were prepared with similar nickel loading and different Mo contents (**Table 1**). The samples with low, medium, and high molybdenum loadings are denoted hereafter as $NiMo_{(L)}$/Z-1(2), $NiMo_{(M)}$/Z-1(2), and $NiMo_{(H)}$/Z-1(2), respectively.

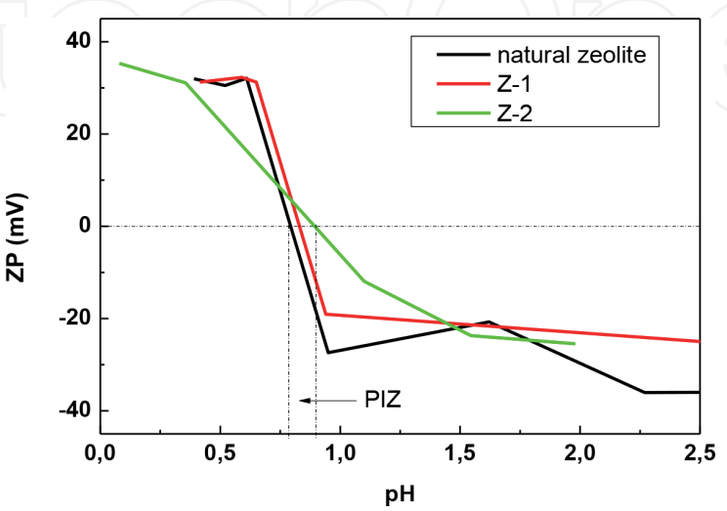

Figure 1.
Isoelectric points (PIZ) of the clinoptilolite *zeolite modified by leaching with HNO_3 during different times (24 and 48 h).*

Sample	Ni (wt.%)	Mo (wt.%)	Support treatment	Total acidity[a] (μmol NH_3/g)
Ni-$Mo_{(L)}$/Z-1	1.19	8.16	HNO_3/24 h	0.18 (0.14)
Ni-$Mo_{(L)}$/Z-2			HNO_3/48 h	0.23 (0.11)
Ni-$Mo_{(M)}$/Z-1	1.64	11.3	HNO_3/24 h	0.18 (0.14)
Ni-$Mo_{(M)}$/Z-2			HNO_3/48 h	0.27 (0.11)
Ni-$Mo_{(H)}$/Z-1	2.82	19.43	HNO_3/24 h	0.10 (0.14)
Ni-$Mo_{(H)}$/Z-2			HNO_3/48 h	0.12 (0.11)

[a] *Acidity data of the substrates are given in parenthesis.*

Table 1.
Catalyst codes, nominal metal loadings, and total acidity (from TPD-NH_3) of the calcined Ni-Mo(x)/ Clinoptilolite *samples.*

2.3 Characterization techniques

The isoelectric points (PIZ) of the *clinoptilolite* zeolite modified with different treatments were measured on a Zeta-Meter System 3.0 containing a cell electrophoretic acrylic type II-grape and platinum electrodes. Surface morphology analysis of the pure zeolites and oxide catalysts precursors was studied by SEM technique using a JEOL JSM-6060 LV microscope. The accelerating voltage employed was 15 kV. Elemental analysis was performed by Energy Dispersive X-ray Spectroscopy (EDS) Oxford Inca X-Sight coupled to a MT 1000, Hitachi apparatus. The textural properties of the oxide precursors and bare supports were determined from the adsorption-desorption isotherms of nitrogen at −196°C, recorded with an ASAP 2420 Micromeritics V2.09 gas sorption Analyzer. Prior to the experiments, the samples were degassed under a flow of argon at 350°C for 16 h. The acidity of the oxide precursors was determined by temperature-programmed desorption (TPD) of ammonia measurements conducted on a Micromeritics 2900 equipment provided with a TCD and interfaced to a data station. The morphology of fresh sulfided catalysts was investigated by high resolution transmission electron microscopy (HRTEM) using a JEOL JEM 2000FX microscope. XPS spectra of the sulfided (10% H_2S in H_2, 673 K) catalyst samples were measured at room temperature using a VG Scientific LTD system equipped with a hemispherical electron analyzer and a Mg Kα ($h\nu$ = 1253.6 eV) X-ray source and ultrahigh vacuum chamber. Details of the XPS measurements by this spectrometer are reported by Huirache-Acuña et al. [23].

2.4 Catalytic activity measurements

The catalyst activity was evaluated in the reaction of hydrodesulfurization of 3-methyl-thiophene (3MeT) carried out in a micro-flow reactor at 280°C upon atmospheric hydrogen pressure. The reactor was loaded with 100 mg of catalyst (particle size between the 80 and 120 mesh) diluted with 1 g of SiC. Before reaction, the catalyst was pre-sulfided at 400°C for 1 h using a gas mixture of 15% H_2S/H_2 (flow rate of 40 mL/min). After catalyst activation, the sample was cooled down and stabilized at reaction temperature. Then, the saturation of hydrogen with 3MeT was obtained by bubbling hydrogen (70 mL min^{-1}) through a saturator containing 3MeT liquid at 20°C. The flow of 3-MeT through reactor was 1.134×10^{-6} moles × s^{-1}. The products obtained at steady state conditions were analyzed on line by GC. For each catalyst studied, steady state conditions were reached after 1 h of time on-stream reaction. All reaction products were analyzed online with gas chromatograph Agilent-7820, FID equipped with an Agilent 30 m HP-5 capillary column. The catalytic activity was expressed as total 3-MeT conversion obtained at steady-state conditions.

3. Results

3.1 Physicochemical characterization of oxide precursors

The surface morphology of the pure Z-1 and Z-2 zeolites and their respective oxide catalyst precursors were investigated by scanning electron microscopy (SEM). The SEM micrographs in **Figure 2** illustrate the influence of the different zeolite pretreatment conditions and Mo loading on the particle size and morphology of the prepared catalysts. In general, irrespectively of the time of HNO_3 treatment (24 or 48 h), both pure Z-1 and Z-2 substrates exhibit irregular and compact structure with white points resulting from the different cations impurities. After Ni and Mo oxide loading, all samples exhibit non-uniform distribution of Ni and Mo on the catalyst surface. The $NiMo_{(H)}$/Z-1 appeared to have a much better distribution of the metal oxides on the support surface than its Z-2-supported counterpart. Besides its highest metal oxide loadings, the surface of both $NiMo_{(H)}$/Z-1 and $NiMo_{(H)}$/Z-2 catalysts were not completely covered with Ni and Mo oxides. This was confirmed by the energy-dispersive X-ray spectroscopy (EDS) analysis on the different points of the samples. SEM/EDS have shown that $NiMo_{(H)}$/Z-1 and $NiMo_{(L)}$/Z-2 samples are characterized by the high Al/Si ratio (5.5 and 4.7, respectively), which might indicate that mean crystalline phase is *clinoptilolite* [3].

The textural properties of pure Z-1 and Z-2 substrates and both oxide catalysts with highest Mo loading was studied by the N_2 physisorption at −196°C. The N_2 adsorption-desorption isotherms of both parent zeolites were similar before and after metal loadings. **Figure 3(A)** shows the N_2 isotherms of both catalysts. According to IUPAC classification, all samples exhibit a combination of a type I and IV isotherms which are typical for hierarchical materials having both micro- and meso-porous structure [24]. Indeed, the H4-type of hysteresis loop is generally observed with complex materials containing both micropores and mesopores [24]. The adsorption branch of N_2 isotherm, which does not show any limiting adsorption at high P/P_0, is typical for natural zeolites having both micro- and meso-pores [3]. However, in case of natural zeolites, an increase of the relative pressure might favor also multilayer adsorption of nitrogen on the surface of impurities [3].

The natural acid-modified *clinoptilolite* zeolite contains micropores, as deduced from the shape of the N_2 sorption isotherms (**Table 2**). However, the relatively low volume of micropores (in range 0.002–0.011 $cm^3 \cdot g^{-1}$) point out that their large amount cannot be detected because the micropores are occupied by exchangeable cations [2].

As expected, an increase of leaching time of pristine zeolite from 24 to 48 h led to an increase of specific surface area (S_{BET}) from 44 to 55 $m^2 \cdot g^{-1}$ and the total pore volume from 0.066 to 0.071 $cm^3 \cdot g^{-1}$ (**Table 2**). Simultaneously, the two-fold increase of volume of micropores occurs (from 0.006 to 0.011 $cm^3 \cdot g^{-1}$) suggesting that the nitrogen access was enhanced by elimination of blocking of the pores by impurities. However, the BET specific area and total pore volume decreased again after metal loading onto surface of zeolite. In addition, the micropore volume decreases after metal oxide incorporation into both Z-1 and Z-2 supports suggesting the modification of pore opening by deposition of the large amount of the Mo species on the carrier surface (**Table 2**).

Figure 3(B) shows the pore size distributions (PSD) evaluated from the adsorption branch of nitrogen isotherm by using BJH method. For all catalysts, pore size distribution shows two distinct peaks: the first one, located about 3.6 nm, is due to the *tensile strength effect* (TSE) [25]. The second broad peak centered at 9.5 and 20.9 nm for $NiMo_{(H)}$/Z-2 and $NiMo_{(H)}$/Z-1, respectively, represents the

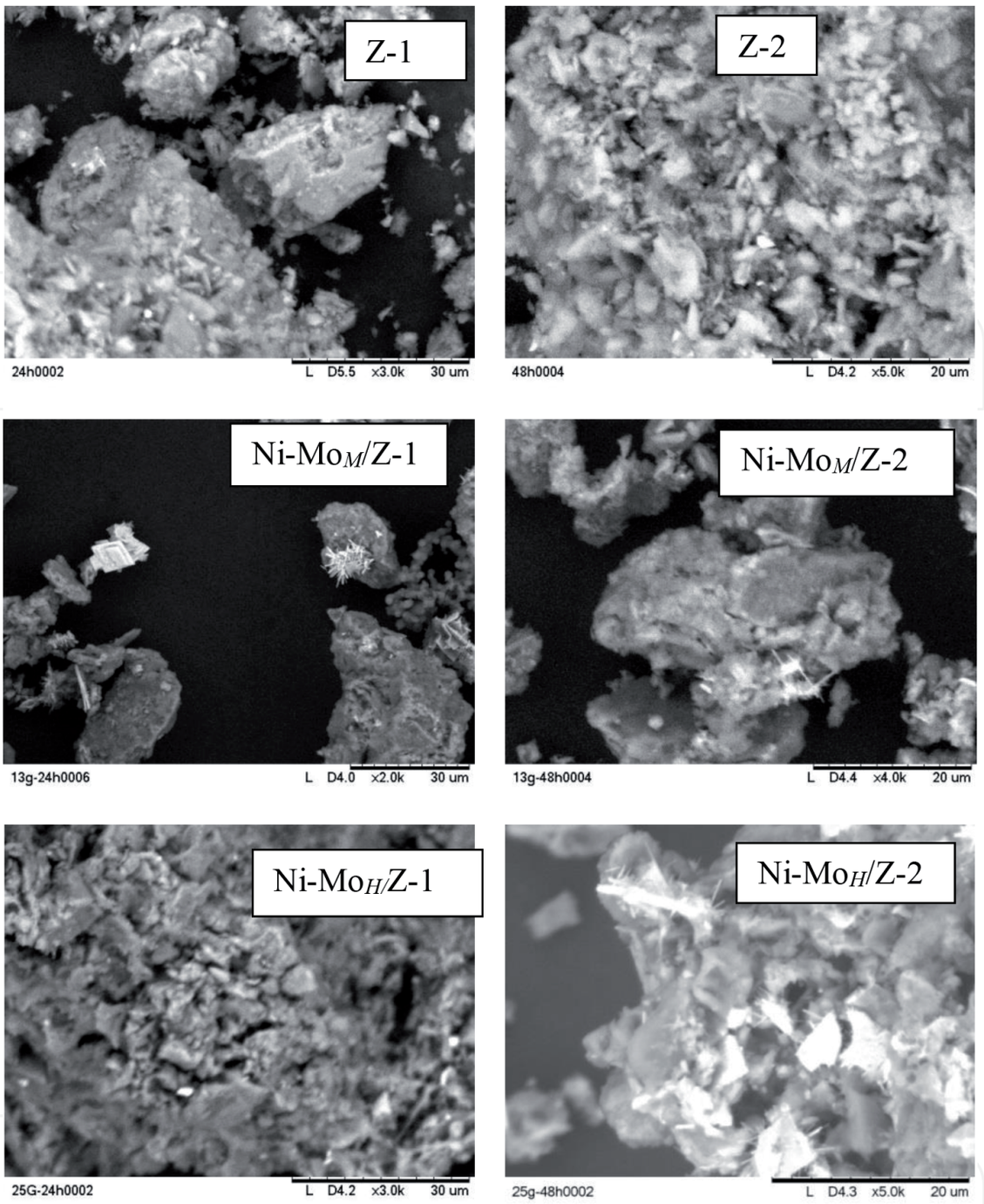

Figure 2.
SEM images of pure Z-1 and Z-2 zeolites and selected oxide catalysts' precursors.

mesopores, probably intra particle porosity [26]. Noticeably, the contribution of the mesoporosity to overall catalyst porous structure is small being all catalysts mainly microporous, as deduced from the comparison of the V_{total} and V_{micro} values in **Table 2**. A comparison of the loss of S_{BET} and normalized S_{BET} values of the calcined $NiMo_{(H)}$/Z-1 catalyst with that of $NiMo_{(H)}$/Z-2 strongly suggest that the former catalyst exhibits a lower pore occlusion by guest molecules than the latter.

The acidity of the calcined catalysts was studied by temperature-programmed desorption of ammonia (TPD-NH_3). The TPD-NH_3 profiles of the most active catalysts are shown in **Figure 4**. Depending on the ammonia desorption temperature, the TPD-NH_3 profiles were mathematically fitted (Gaussian function) assuming temperature desorption ranges of 100–250°C, 250–400°C and 400–500°C, respectively, as indicative of weak, medium, and strong strength acid sites [27]. The

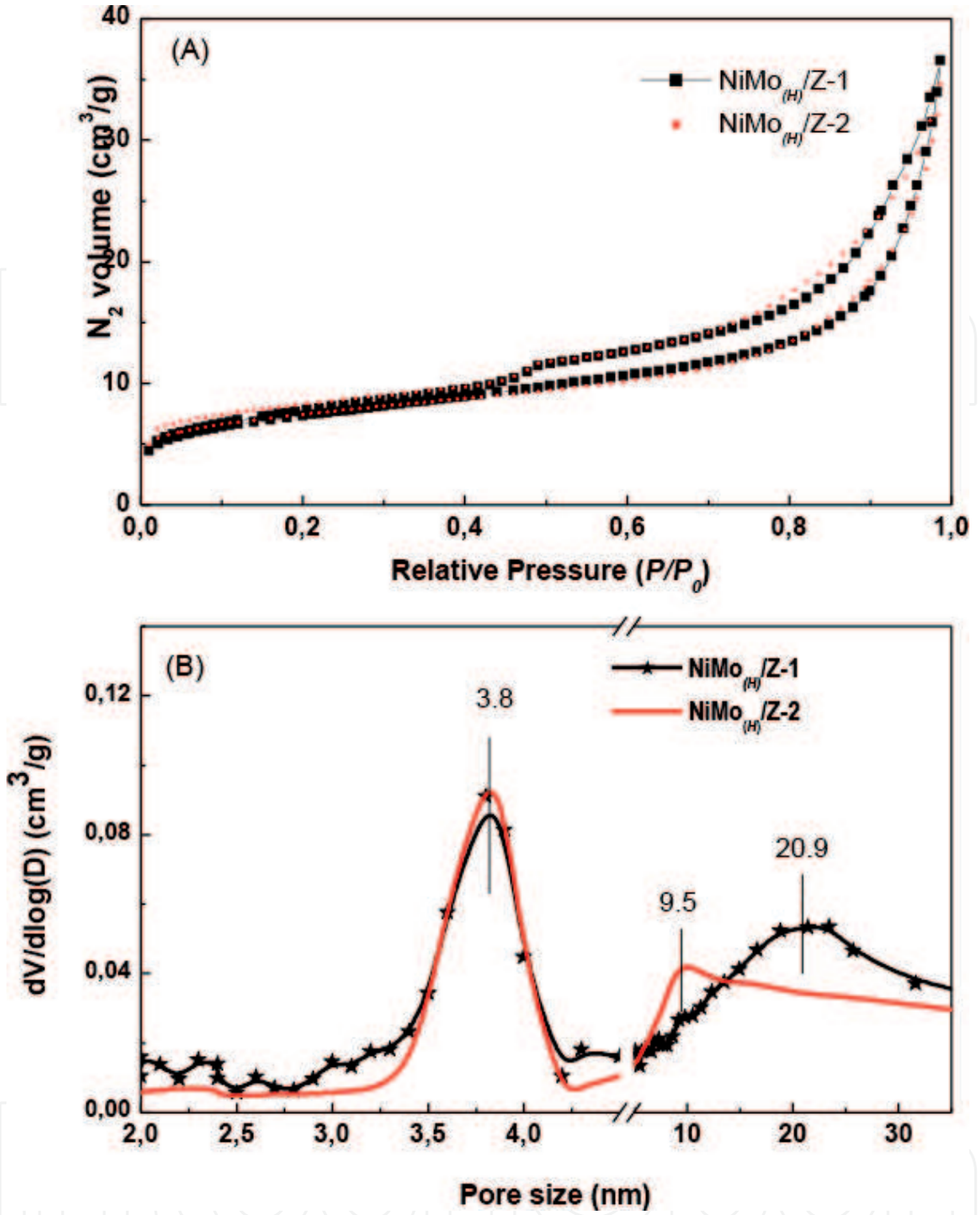

Figure 3.
N2 adsorption-desorption isotherms of the calcined Ni-Mo$_{(H)}$/Z-1(Z-2) catalysts (A) and their BJH adsorption pore size distribution (B).

weak and moderate acidity are probably linked with Brønsted acid sites, whereas the strong acid sites are probably originated by Lewis acid sites [28, 29]. As seen in **Figure 4**, the Ni-Mo$_{(L)}$/Z-2 and NiMo$_{(M)}$/Z-2 catalysts exhibited a larger amount of strong strength acid sites than their Z-1-supported counterparts suggesting the poorer metal oxides dispersion on the surface of those catalysts. The total concentration of acid sites (expressed as μmol_{NH3} per g of substrate) is shown in **Table 1**. In general, the catalysts supported on Z-2 zeolite exhibit larger total acidity than their counterparts supported on Z-1 zeolite. The total acidity of the oxide precursors follows the trend: NiMo$_{(M)}$/Z-2 ≈ NiMo$_{(L)}$/Z-2 >> others. Irrespectively of the support, the strong acid sites disappeared after loading the largest Mo amount. According to Del Arco et al. [26], XRD measurements suggest that this is probably due to

Materials	S_{BET} ($m^2\ g^{-1}$)	Loss of S_{BET} [b] (%)	N_{SBET}	V_{total} ($cm^3\ g^{-1}$)	V_{micro} ($cm^3\ g^{-1}$)	d_p (nm)
Z-1	44	—	—	0.066	0.006	8.1
$NiMo_{(H)}$/Z-1	25	43	0.75	0.049	0.003	9.2
Z-2	55	—	—	0.071	0.011	7.6
$NiMo_{(H)}$/Z-2	25	54	0.58	0.046	0.004	10.1

[a] *Specific BET surface area (S_{BET}), total pore volume (V_{total}), micropore volume (V_{micro}) obtained from t-plot; BJH adsorption average pore diameter (d_P).*
[b] *Loss of S_{BET} after metal loading.*
[c] *Normalized specific BET surface area calculated using the equation: NS_{BET} = S_{BET} of catalyst/[(1 − y) × S_{BET} of support] where S_{BET} is the specific BET surface area of the catalyst or support, and y is the weight fraction of the guest phases.*

Table 2.
*Textural properties[a], loss of S_{BET}[b] and normalized S_{BET}[c] of the calcined Ni-Mo(x)/*Clinoptilolite *catalysts.*

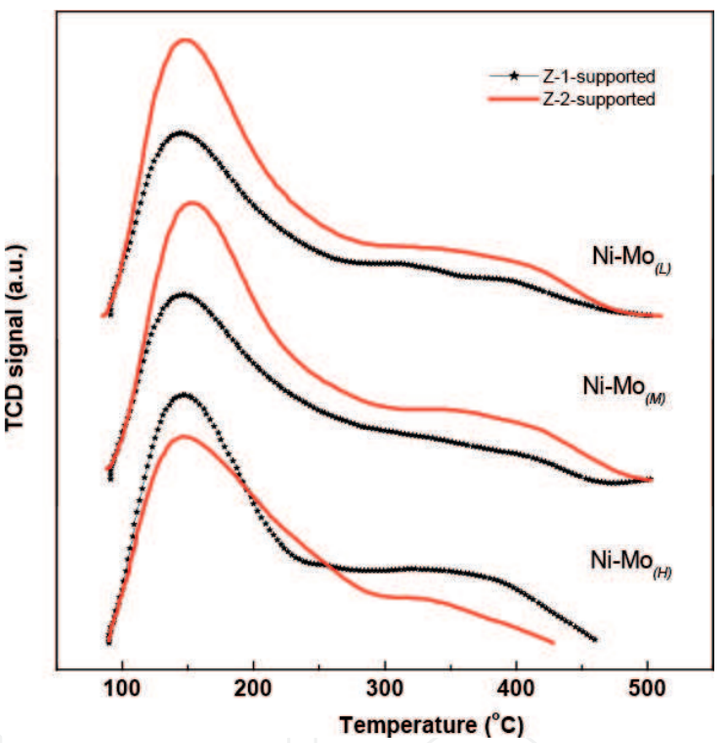

Figure 4.
*TPD-NH_3 profiles of the calcined $NiMo_{(x)}$/*Clinoptilolite *catalysts.*

formation of large MoO_3 crystallites on the support surface affecting the acidity associated with surface –OH groups.

Summarizing, taking in account all characterization data of the oxide catalyst precursors, zeolite leaching with HNO_3 during 24 h led to better support than its leaching during 48 h. This is probably because an increase of leaching time increased the support microporosity leading to a decrease of the average pore diameter (**Table 2**). After zeolite leaching and further metal loading, the structure of zeolite material was maintained, as confirmed by XRD studies by Khoshbin et al. [5]. SEM mapping analysis confirmed that main part of the metal ion impurities of natural zeolite had been displaced by H^+ ions after zeolite leaching with HNO_3 solution at 24 and 48 h. $NiMo_{(H)}$/Z-1 was the only catalyst having K^+ impurities on its support surface, as confirmed by SEM mapping (data not shown here) and chemical surface analysis by XPS (*vide infra*). Finally, the zeolite leaching with HNO_3 led to modification of the number of acid sites and their strength, as confirmed by TPD-NH_3 analysis, being more acidic the catalysts supported on zeolites leached during 24 h (**Table 1**).

3.2 Characterization of freshly sulfided catalysts

3.2.1 TEM characterizations

The HRTEM micrographs of both sulfided catalysts with highest Mo content are compared in **Figure 5**. Noticeably, the $NiMo_{(H)}$/Z-1 exhibit a larger density of Mo sulfide particles on the surface of Z-1 zeolite than its $NiMo_{(H)}$/Z-2 counterpart. The molybdenum sulfide particles on the surface of Ni-$Mo_{(H)}$/Z-1 catalyst are relatively large, and they are formed with slabs presenting a high degree of stacking faults. As seen, the slabs of the molybdenum sulfide are partially intercalated by other slabs. The interlayer spacing of 0.61 nm observed from lattice fringes can be ascribed to the (002) direction of the bulk MoS_2. However, SEM mapping of this sample (not shown here) indicated the presence of both Mo and S elements with concentration suggesting the formation of $MoS_{1.95}$ phase. For the $NiMo_{(H)}$/Z-1, the statistical analysis of about 250 particles of various HRTEM images reveals that this sample exhibits MoS_2/$MoS_{1.95}$ particles with an average size of 6.3 ± 3.1 nm and an average stacking number of about 7.0 (**Table 3**). Noticeably, the $NiMo_{(H)}$/Z-2 exhibit much lower stacking of the MoS_2 slabs than its $NiMo_{(H)}$/Z-1 counterpart (see **Figure 5(B)** and **Table 3**). Thus, both catalysts might exhibit different amounts of Mo atoms in the edge surface of molybdenum sulfide crystals [30]. To confirm this, the average fraction of Mo atoms in the edge surface of MoS_2/$MoS_{1.95}$ crystals was calculated (see f_{Mo} and f'_{Mo} values in **Table 3**) following the method used by Gutierrez and Klimova [31]. The comparison of the f'_{Mo} values, in which the layer attached to the support surface is not considered, clearly indicated that Z-1-supported catalyst contains a larger amount of those Mo atoms in the edge surface of the MoS_2/$MoS_{1.95}$ crystals than its Z-2-supported counterpart.

Noticeably, both Z-1 supported catalysts with high and medium Mo contents exhibit very similar f'_{Mo} values (**Table 3**) suggesting that the amount of Mo atoms in the edge surface of the active phase can be due to specific properties of the Z-1 support. Indeed, contrary to the Ni-$Mo_{(H)}$/Z-1 catalyst, the MoS_2 fringes of the Ni-$Mo_{(H)}$/Z-2 catalyst exhibit strong bending effect (**Figure 5**). Similar bending effect can be seen in **Figure 6** showing the HRTEM image of the Ni-$Mo_{(M)}$/Z-2 sulfide catalyst with a typical SAED pattern evidencing diffraction rings of the crystalline MoS_2 phase. The HRTEM image of this sample, the MoS_2 layers are disordered,

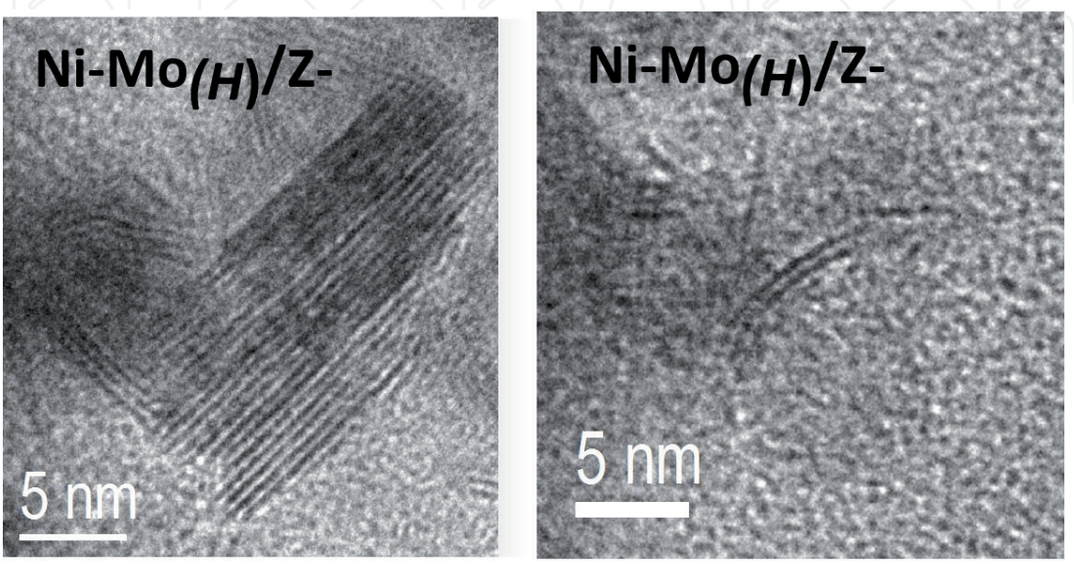

Figure 5.
HRTEM images obtained for fresh sulfided Ni-$Mo_{(H)}$/Z-1 (A) and Ni-$Mo_{(H)}$/Z-2 (B) catalysts.

Sample	*L* (nm)	*N*	f_{Mo}	f'_{Mo}
$NiMo_{(H)}$/Z-1	6.3 ± 3.1	7.0 ± 5.4	0.19	0.17
$NiMo_{(H)}$/Z-2	6.0 ± 3.6	1.2 ± 1.1	0.20	0.03
$NiMo_{(M)}$/Z-1	6.9 ± 3.8	8.4 ± 7.9	0.18	0.16

[a]MoS_2 particle size: length (L) and number of slabs (N); f_{Mo} is average fraction of Mo atoms in the edge surface of the MoS_2 crystals; f'_{Mo} is f_{Mo} value in which the layer attached to the support was not considered [31] .

Table 3.
Some HRTEM data[a] of the selected sulfided catalysts.

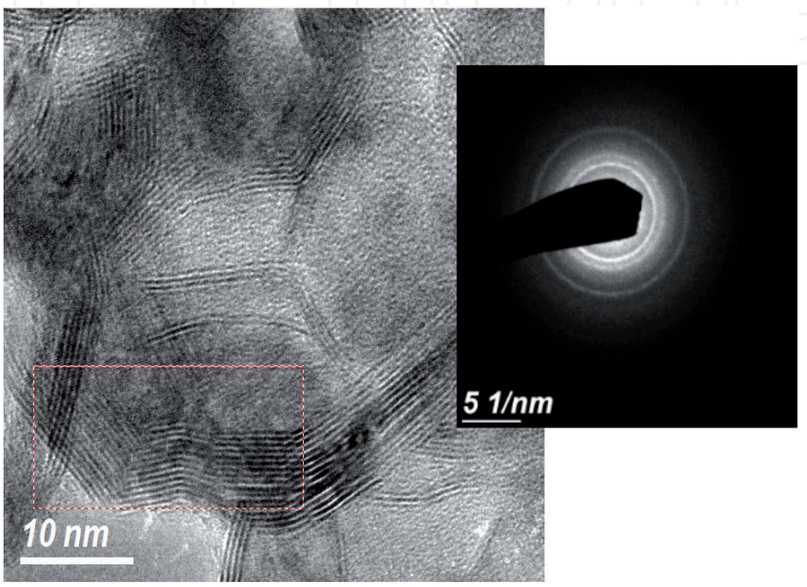

Figure 6.
High resolution TEM images of the Ni-$Mo_{(M)}$/Z-2 sulfide catalyst showing MoS2 fringes with a strong bending effect. Layers are disordered, highly stacked, and broken at the point of highest torsion. Inset: FFT analysis over the area marked by the dotted squares in panel evidencing polycrystalline structure of a large particle.

highly stacked and broken at the point of highest torsion. It is hypnotized that this can be due to the presence of impurities on the surface of Z-2 zeolite forcing the formation of the "onion-type" MoS_2 phase.

3.2.2 X-ray photoelectron spectroscopy (XPS)

Since the objective of the zeolite leaching was unblocking of its channels through dealumination and decationation, the surface exposure of undesired elements of the fresh sulfided catalysts was evaluated by XPS. For all fresh sulfided catalysts, the binding energies (BE) of same components of the zeolite carrier were: Si 2p (103.4 eV), Al 2p (74.5–75.0 eV), Fe $2p_{3/2}$ (710.6–711.1 eV), and F 1 s (685.5–685.8 eV). Interestingly, the Si 2p core level peak of all samples was close to 103.4 eV, which is characteristic of O-Si-O bonds in SiO_2. Thus, the chemical environment of silicon ions was not affected by the presence of Al^{3+}, Fe^{3+}, F^-, and K^+ ions. Considering data shown in **Table 4**, the impurities present on the support surface can be K_2O, Al_2O_3, Fe_2O_3, and SiF_4. The surface exposure of the Al^{3+} ions on the Z-1 zeolite decreases according at the trend: Ni-$Mo_{(L)}$/Z-1 > Ni-$Mo_{(M)}$/Z-1 > Ni $Mo_{(H)}$/Z-1.

The sulfiding behavior of Ni and Mo on the *clinoptilolite*-supported catalysts was investigated by in situ XPS. The effect of support was evaluated by comparison of the sulfiding behavior of $NiMo_{(H)}$ samples, whereas the effect of

Sample	Al/Si at	K/Si at	Fe/Si at	F/Si at	(Al + Fe + F)/Si
$NiMo_{(L)}$/Z-1	0.217	—	0.054	0.096	0.367
$NiMo_{(M)}$/Z-1	0.198	—	0.056	0.051	0.305
$NiMo_{(H)}$/Z-1	0.126	0.029	0.058	0.053	0.237
$NiMo_{(H)}$/Z-2	0.145	—	0.051	0.051	0.247

Table 4.
Surface atomic ratios of the undesired elements of the Clinoptilolite*-based NiMo sulfide catalysts.*

Catalysts	$Mo3d_{5/2}$	$Ni\ 2p_{3/2}$	S 2p
$NiMo_{(L)}$/Z-1	228.9	852.4 (40)	161.9
		855.8 (60)	
$NiMo_{(M)}$/Z-1	228.9	853.2 (40)	161.8
		856.0 (60)	
$NiMo_{(H)}$/Z-1	228.8	853.2 (40)	161.6
		856.0 (60)	
$NiMo_{(H)}$/Z-2	229.0	852.5 (38)	161.8
		855.7 (62)	

[a]*In parentheses are peak percentages.*

Table 5.
Binding energies (eV) of core electrons[a] of Clinoptilolite*-based NiMo sulfide catalysts.*

Mo loading was evaluated by comparison of the Z-1-supported catalysts. The binding energies (eV) of the principal peaks are summarized in **Table 5** and the percentages of different species are given in parentheses. Concerning the Mo 3d core level spectra (not shown here), two doublet peaks containing the corresponding $3d_{5/2}$ and $3d_{3/2}$ components from the spin-orbit splitting suggested the presence of two types of molybdenum species. For all catalysts, the lower Mo $3d_{5/2}$ binding energy at 228.5–228.8 eV is similar to that reported for Mo_2S_3 phase (228.7 eV) with a Mo oxidation state of +3 [32]. Noticeably, the binding energy of the S $2p_{3/2}$ peak observed for the $NiMo_{(H)}$ catalysts at 161.6–161.9 eV is a little too low to be considered of sulfide (S^{2-}) ions present in the MoS_2 phase (162.4 eV) [33]. Thus, regardless of the support (Z-1 or Z-2) and Mo loading, the XPS results suggest that the sulfidation of molybdenum species located on the support surface is complete. Conversely to Mo, an important proportion of nickel species remains unsulfided, as deduced from two contributions of the Ni $2p_{3/2}$ component: one at 852.6–853.2 eV associated with nickel sulfide species and another one at 855.9–856.0 eV due to oxidized Ni^{2+} ions [34]. The comparison of the relative intensities of the Ni $2p_{3/2}$ peaks of sulfided and unsulfided Ni species in all samples suggests the similar degree of sulfidation of Ni^{2+} in all samples (40%). The $NiMo_{(H)}$/Z-2 sample is only one showing a little lower Ni species sulfidation degree (38%). Thus, the final state of sulfidation of the catalysts was independent on the support and molybdenum loading.

Concerning the effect of support, the comparison of the Mo/Si, Ni/Si, and S/Si atomic ratios of $NiMo_{(H)}$/Z-1 and $NiMo_{(H)}$/Z-2 catalysts clearly indicated that a better Mo and Ni species surface exposure was achieved using Z-2 as support (see Mo/Si and Ni/Si atomic ratios in **Table 6**). This is not surprising because Z-2 exhibits a larger specific surface area than Z-1 (55 m^2/g vs. 44 m^2/g). By comparison of surface atomic ratios of the impurities in the Z-1 and Z-2 catalysts, one can notice higher impurities of the Z-2-based catalysts.

Sample	Mo/Si at	Ni/Si at		$(Ni + Mo)_{(s)}/Si$	S/Si at	$S/(Ni + Mo)_{(S)}$	S/Mo
		Ni-O	Ni-S				
$NiMo_{(L)}$/Z-1	0.049	0.014	0.009	0.058	0.116	2.0	2.04
$NiMo_{(M)}$/Z-1	0.174	0.024	0.016	0.190	0.445	2.3	2.30
$NiMo_{(H)}$/Z-1	0.080	0.010	0.007	0.087	0.177	2.0	2.06
$NiMo_{(H)}$/Z-2	0.160	0.027	0.016	0.176	0.393	2.2	2.31

Table 6.
Surface atomic ratios of active phases for the Clinoptilolite*-based NiMo sulfide catalysts.*

In contrast to Mo species, the XPS results suggest that Ni species are partially sulfided. Considering the catalyst sulfidation degree, the comparison of the S/(Ni + Mo) ratios of both catalysts strongly suggest that, on the contrary to $NiMo_{(H)}$/Z-2 catalyst, the $NiMo_{(H)}$/Z-1 exhibits non stoichiometric molybdenum sulfide phase. Contrary to Z-1 supported catalysts, the results of the XPS analysis show that the S:Mo ratio on the samples supported on Z-2 zeolite is higher than that found for MoS_2 (**Table 6**). The excess of sulfur in those samples corresponds to elemental sulfur. This is important observation because it can explain the much better catalytic response of the $NiMo_{(H)}$/Z-1 sample with respect its Z-2 supported counterpart.

In conclusion, the interpretation of the catalyst structure by XPS results appears more straightforward than by HRTEM. The main reason for difficulty of the catalyst characterization by the latter technique is related to the fact that many impurities are still present of the catalyst surface after zeolite leaching with HNO_3 which leads to a limited number of TEM zones where molybdenum and nickel sulfides are both clearly visualized.

3.2.3 Hydrodesulfurization of gasoline model compound

The current desulfurization technology for gasoline production requires highly selective catalysts to remove S-compounds without excessive olefins hydrogenation. The latter requirement is especially important for preservation of the research octane number (RON) [1, 2]. Thus, the catalyst needed to the hydrotreating of naphtha stream needs to possess moderate hydrogenation properties. In this work, the activity and selectivity of the sulfided $NiMo_{(x)}$/*Clinoptilolite* catalysts were evaluated in the hydrodesulfurization (HDS) of 3-methylthiophene (3-MeT) as gasoline model compound. The reaction was carried out in a flow reactor under atmospheric hydrogen pressure and reaction temperature of 280°C. The 3-MeT conversion was low (0.8–5.3%) in order to avoid diffusional problems and to compare the catalysts under kinetic conditions. The intrinsic 3-MeT HDS activities at 360°C of the $NiMo_{(x)}$/Z-1 and $NiMo_{(x)}$/Z-2 catalysts (expressed as moles of 3-MeT converted per second and gram of catalyst), under steady-state conditions and reaction temperature of 280°C, are compared in **Figure 7(A)**. The specific reaction rate of the best catalyst ($NiMo_{(H)}$/Z-1) was close to that of Ni-W/SiO_2 (60×10^{-8} mol_{3MT} g^{-1} s^{-1} vs. 70×10^{-8} mol_{3MT} g^{-1} s^{-1}) tested at the same reaction temperature (280°C) [35].

Regardless of the support and metal loading, the reaction products identified by GC were; 3-methyltetrahydrothiophene (3MTHT); 2-methylbutane-1-thiol (2MBT1); 2-methyl-1,3-butadiene (isoprene); 3-methyl-1-butene (3M1B); 2-methyl-1-butene (2M1B); and 2-methyl-2-butene (2M2B). The main products detected were 2-methyl-1-butene and isoprene. The HYD/DDS selectivities ratios of the catalysis are compared in **Figure 7(B)**. Noticeably, the hydrogenation of olefins to paraffin's did not occur because 2-methyl-1-butane (2 MB) was not produced. The

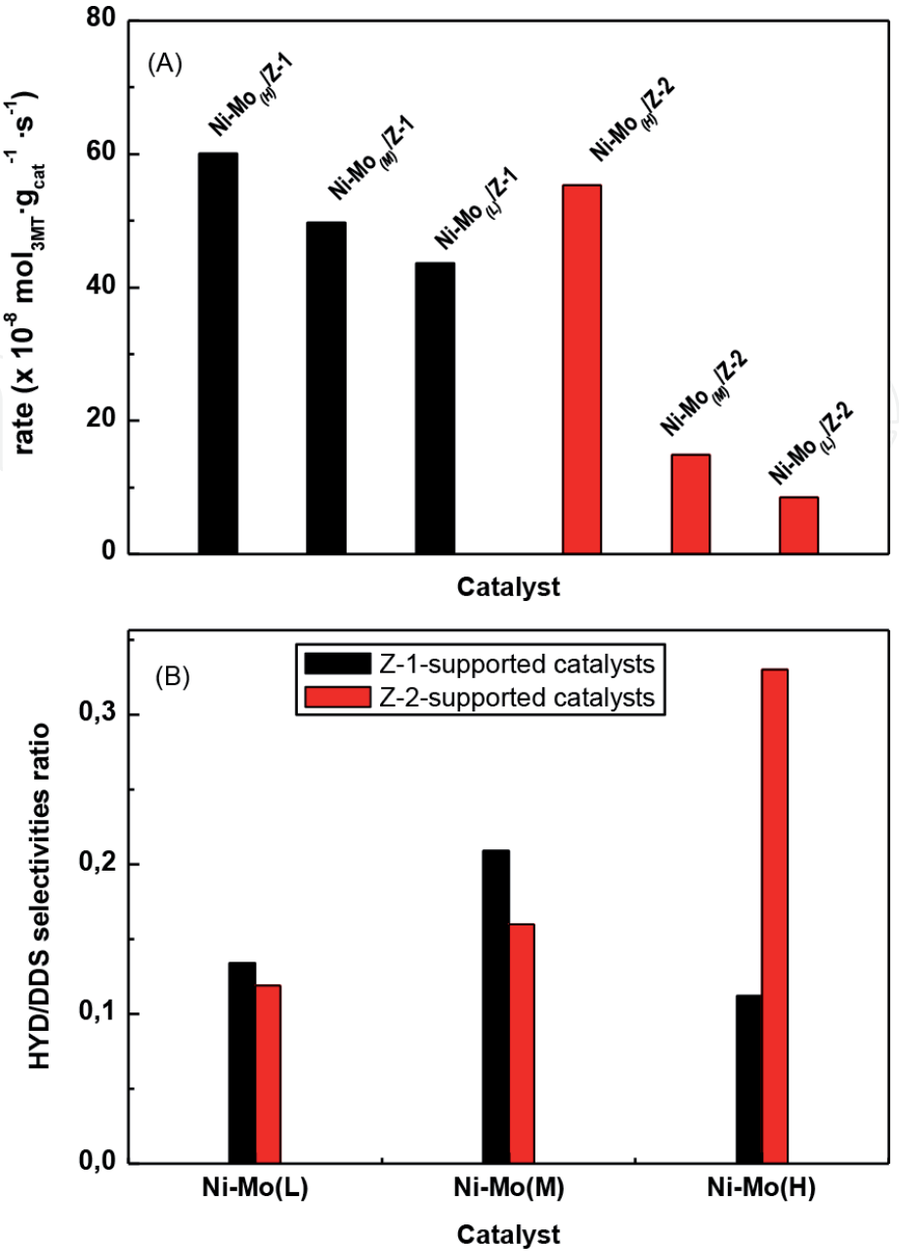

Figure 7.
*Steady state reaction rates (A) and HYD/DDS selectivities ratio (B) for HDS of 3MeT (flow reactor, T = 280°C; atmospheric H2 pressure) over sulfide NiMo$_{(x)}$/*Clinoptilolite *catalysts.*

possible reaction path network for the HDS of 3MeT over catalysts studied is shown in **Figure 8**. As seen in **Figure 8** the 3-MeT transformation occurs via hydrogenation (HYD) and direct desulfurization (DDS) reaction routes. Considering the first HYD step, the double bond of 3MeT is saturated leading to formation of 3-methyl-2,3-dihydrothiophene (3M2,3DHT). This product was not detected in this work because it was quickly transformed to 3-methyl-tetrahydrothiophene (3-MTHT) and then to a mixture of 2-methyl-butane-1-tiol (2M1BT) and 3-methyl-butane-1-tiol (3M1BT) products. On the other hand, the DDS path leads to the formation of isoprene and its subsequent transformation to mixture of olefins (3M1B, 2M1B, and 2M2B). Interestingly, the formation of 2-methylbutane via hydrogenation olefins did not occur. It is important finding of this work because such hydrogenation is not desired reaction during hydroprocessing of naphtha feedstocks.

Contrary to the NiW supported on SiO_2 and γ-Al_2O_3 [35], the formation of pentenes via isomerization of the olefin mixture compounds (3M1B, 2M1B, and 2M2B) was not observed in this work. The formation of mixed olefin compounds (3M1B,

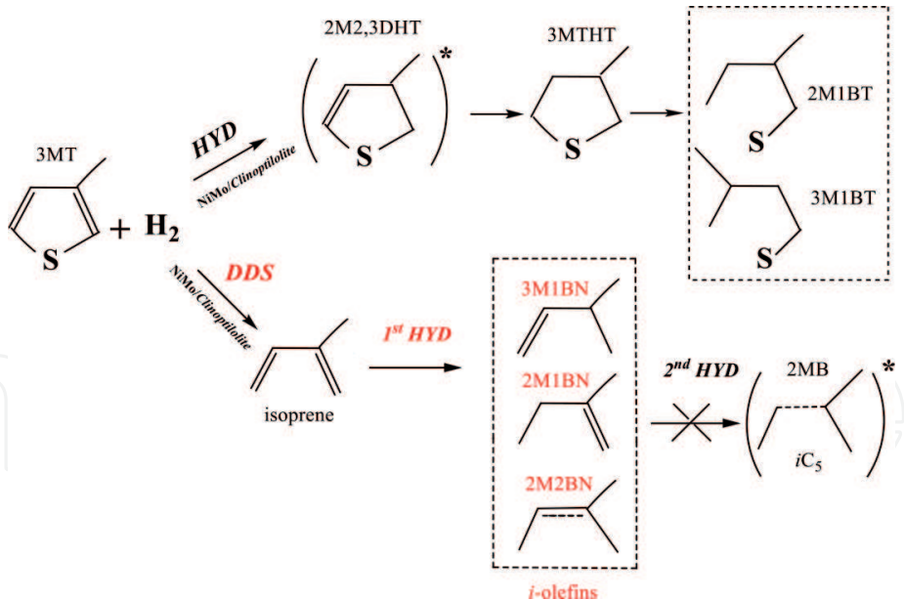

Figure 8.
*Reaction path network for the 3-methyl-thiophene (3MeT) transformation over NiMo/*Clinoptilolite *sulfide catalysts.*

2M1B, and 2M2B) was higher over the NiMo catalysts supported on Z-1 zeolite than over the counterpart Z-2 zeolite. In general, the Z-1-supported catalysts exhibit a larger formation of those mixed olefins than their counterparts supported on Z-2. Noticeably, none of the catalyst studied exhibited the formation of totally hydrogenated products. This fact is of paramount importance for production of FCC gasoline which needs the sulfur removal without excessive olefin saturation. In general, all catalysts exhibit a decrease in HYD selectivity with increasing 3-MeT conversion, as it was observed previously for sulfided Ni-Mo catalysts supported on silica-alumina [36]. This means that in the absence of thermodynamic effects, the hydrogenolysis of 3-MeT is more favorable than hydrogenation of aromatic ring. By comparing the activity and HYD/DDS selectivities ratio of the $NiMo_{(H)}$/Z-1 and $NiMo_{(L)}$/Z-1 samples in reaction at 280°C, it is clear that the increase of Mo loading led to increase of 3-MeT conversion but without changing the HYD/DDS selectivity ratio (**Figure 7(B)**). Interestingly, the largest HYD/DDS selectivities ratio is found by catalysts supported on zeolite *Clinoptilolite* leached during 48 h than their counterparts leached at 24 h.

4. Catalyst activity structure-correlation

The above activity results demonstrated clearly that the best catalyst was that prepared with largest Mo loading and supported on Z-1 carrier ($NiMo_{(H)}$/Z-1). This raise the question of why this catalyst shows higher HDS activity than its counterpart $NiMo_{(H)}$/Z-2 despite their similar nickel and molybdenum contents. To answer this question, the oxide precursors and fresh sulfided catalysts were characterized by different techniques to investigate their morphology, textural properties, acidity, and sulfidability.

In this work, the necessity of natural zeolite modification by leaching was clearly demonstrated. The objective of such leaching was to open porous structure of the natural zeolite by elimination of undesirable cations occluding the pores. For all catalysts studied, the zeolite leaching with HNO_3 during 24 h led to much better support material than its leaching during 48 h. In this sense, the pore size distribution (from N_2 physisorption measurements) confirmed that an increase of leaching time from 24 to 48 h led to an increase of the support mesoporosity, clearly observed

in the 5–35 nm region of the pore size distribution (**Figure 2(A)**). Both Ni and Mo sulfide phases are poorly dispersed and distributed mainly on the external zeolite surface (from XPS), although small amounts of molybdenum sulfides can be also located within the internal support porous structure. The selected zeolite leaching conditions were not so strong in order to avoid destruction of the zeolite structure. Unfortunately, the XPS characterization confirmed that using those mild leaching conditions (HNO_3, 80°C, 24/48 h), it was impossible to eliminate totally Al^{3+}, K^+, Fe^{3+}, and F^- ions from the internal porous structure of the *Clinoptilolite* zeolite. In this sense, it was observed that not all ions have inhibition effect on the catalyst activity.

The higher activity shown by Ni-$Mo_{(H)}$/Z-1 can be attributed to the lowest amount of extraframework (EXFAL) Al atoms occluded in the internal cavities of, as shown by lowest Al/Si atomic ratio among the catalysts studied (**Table 4**). Interestingly, the 3-MeT conversion at 280°C decreased linearly with an increase of Al/Si atomic ratio of Z-1-supported samples. This is probably because the occlusion of Al atoms in the cavities of zeolite increased the catalyst acidic properties favoring the catalyst deactivation induced by acid sites. The best catalytic response of the $NiMo_{(H)}$/Z-1 catalyst can be linked also to the presence of K^+ cations decorating support surface, as this was unique sample among all catalysts studied having K^+ ions on the support surface (**Table 4**). Similar observation was reported previously for the CoMo HDS catalysts supported on aluminosilicate doped with Na [37]. In addition, the presence of potassium species on the catalyst surface might increase the dispersion of Mo phase as well as to influence the coordination state of Mo^{6+} and Ni^{2+} ions in this sample, as it was observed by Raman spectroscopic study [38]. In this sense, it was found that the Ni-Mo/γ-Al_2O_3 sample doped with K^+ exhibited a lower amount of polymeric Mo-O species because potassium provoked their partial transformation into monomeric $Mo^{6+}{}_{(Th)}$ ones. The formation of new complex K-Ni-Mo-O species was proposed [38]. In line with this, it has been found that, contrary to tetrahedral nickel species, the formation of octahedral nickel species in the oxide precursor was beneficial for catalyst activity. Finally, the SEM characterization of the fresh sulfided $NiMo_{(H)}$/Z-1 catalyst suggested the formation of the nonstoichiometric $MoS_{1.95}$ phase, which was postulated as be far more active than the stoichiometric MoS_2 [39]. This is because of anionic vacancies in the molybdenum sulfide lattice of the latter compound with respect to the stoichiometric one. Thus, the deliberate synthesis of a nonstoichiometric MoS_2 is desirable. In addition, the $NiMo_{(H)}$Z-1 catalyst contain a larger amount of Mo atoms in the edge surface of the MoS_2/$MoS_{1.95}$ crystals than its Z-2-supported counterpart, as deduced from HRTEM (**Table 3**). As a consequence, the DDS route of 3MeT transformation have been favored without excessive olefins hydrogenation, as deduced from its lowest HYD/DDS ratio among the catalysts studied (**Figure 7(B)**).

5. Conclusions

The HDS of 3-methylthiophene (3MeT) over NiMo sulfide catalysts supported on natural Mexican zeolite (*Clinoptilolite*) modified by treatment with HNO_3 during 24 and 48 h was performed in a flow reactor under atmospheric hydrogen pressure. The best catalyst was the one loaded with a largest Mo wt.% and supported on HNO_3-treated zeolite during 24 h. The HDS activities of the catalysts were clearly influenced by the forms of MoS_2 slabs, being formation of "onion-type" MoS_2 negative for the catalyst activity. Respect to selectivity, the results indicated that catalysts prepared on Z-1 zeolite had lowest hydrogenation ability, in comparison with the counterpart catalysts supported on Z-2 zeolite. The higher olefin formation on catalysts supported on Z-1 zeolite could be interesting for the tailoring novel catalysts since they could be catalysts for the production of gasolines with a greater octane number.

Acknowledgements

Drs. R. Guil-López and B. Pawelec acknowledges the financial support of the Spanish Ministry of Science, Innovation and Universities (Project CTQ2016-76505-C3-1). Dr. R. Huirache-Acuña acknowledges the financial support of CIC-UMSNH 2019-2020 Project.

Conflict of interest

The authors declare no conflict of interest.

Nomenclature

HYD	hydrogenation reaction route
DDS	direct desulfurization reaction route
2 M-3,3-DHT	2-methyl-2,3-dihydrothiophene
3MTHT	3-methyltetrahydrothiophene
2M1BT	2 methyl 1-butanethiol
3M1BT	3-methyl 1-butanethiol
Isoprene	2-methyl-1,3-butadiene
3M1BN	3-methyl 1-butene
2M1BN	2-methyl 1-butene
2M2BN	2-methyl-2-butene
2MB	2-methylbutane

Author details

Cristina Farías Rosales[1], Rut Guil-López[2], Marisol Faraldos[2], Rafael Maya Yescas[1], Trino Armando Zepeda[3], Barbara Pawelec[2*] and Rafael Huirache-Acuña[1*]

1 Facultad de Ingeniería Química, Universidad Michoacana de San Nicolás de Hidalgo, Ciudad Universitaria, Morelia, Michoacán, México

2 Institute of Catalysis and Petroleum Chemistry, CSIC, Madrid, Spain

3 Centro de Nanociencias y Nanotecnología – UNAM, Ensenada, B.C., México

*Address all correspondence to: bgarcia@icp.csic.es and rafael_huirache@yahoo.it

References

[1] Hossein F, Majid V, Touray T. Desulfurization of gas oil by modified clinoptilolite. Iranian Journal of Chemistry and Chemical Engineering. 2007;**26**(2):19-25. DOI: 1021-9986/07/2/19

[2] Korkuna O, Leboda R, Skubiszewska-Zieba J, Vrublevska T, Grunko VM, Ryczkowski J. Structural and physicochemical properties of natural zeolites: Clinoptilolite and mordenite. Microporous and Mesoporous Materials. 2006;**87**: 243-254

[3] Ostrooumov M, Cappelletti P, de' Gennaro R. Mineralogical study of zeolite from new Mexican deposits (Cuitzeo area, Michoacan, Mexico). Applied Clay Science. 2012;**55**:27-35. DOI: 10.1016/j.clay.2011.09.011

[4] Arcoya A, González JA, Travieso N, Seoane XL. Physicochemical and catalytic properties of a modified natural clinoptilolite. Clay Materials. 1994;**29**:123-131

[5] Khoshbin R, Haghighi M, Asgari N. Direct synthesis of dimethylether on the admixed nanocatalysts of CuO-ZnO-Al_2O_3 and HNO_3-modified clinoptilolite at high pressures: Surface properties and catalytic performance. Materials Research Bulletin. 2013;**48**:767-777. DOI: 10.1016/j.materresbull.2012.11.057

[6] Chmielewska E, Pilchowski K. Surface modifications of natural clinoptilolite-dominated zeolite for phenolic pollutant mitigation. Chemical Papers. 2006;**60**:98-101. DOI: 10.2478/s11696-006-0018-8

[7] Barrer RM, Makki MB. Molecular sieve sorbents from clinoptilolite. Canadian Journal of Chemistry. 1964;**42**:1481-1487. DOI: 10.1139/v64-223

[8] Tihmillioglu F, Ulku S. Use of clinoptilolite in ethanol dehydration. Separation Science and Technology. 1996;**31**:2855-2865. DOI: 10.1080/01496399608000832

[9] Abdulkareem SA, Muzenda E, Afolabi AS, Kabuba J. Treatment of clinoptilolite as an adsorbent for the removal of copper ion from synthetic wastewater solution. Arabian Journal for Science and Engineering. 2013;**38**:2263-2272. DOI: 10.1007/s13369-012-0505-x

[10] Yasyerli S, Ar I, Dogu G, Dogu T. Removal of hydrogen sulfide by clinoptilolite in a fixed bed adsorber. Chemical Engineering and Processing. 2002;**41**:785-792. DOI: 10.1016/S0255-2701(02)00009-0

[11] Hutchings GJ, Themistocleous T, Copperthwaite RG. Conversion of propane and butane. US patent 5162598. November 10, 1992

[12] Dziedzicka A, Sulikowski B, Ruggiero-Mikołajczyk M. Catalytic and physicochemical properties of modified natural clinoptilolite. Catalysis Today. 2016;**259**:50-58. DOI: 10.1016/j.cattod.2015.04.039

[13] Allahverdiev AI, Irandoust S, Murzin DY. Isomerization of of α-pinene over Clinoptilolite. Journal of Catalysis. 1999;**185**:352-362. DOI: 10.1006/jcat.1999.2474

[14] Woo HC, Lee KH, Lee JS. Catalytic skeletal isomerization of n-butenes to isobutene over natural clinoptilolite zeolite. Applied Catalysis A: General. 1996;**134**:147-158. DOI: 10.1016/0926-860X(95)00216-2

[15] Lee HC, Woo HC, Ryoo R, Lee KH, Lee JS. Skeletal isomerization of n-butenes to isobutene over acid-treated natural clinoptilolite zeolites. Applied Catalysis A: General. 2000;**196**:135-142. DOI: 10.1016/S0926-860X(99)00458-5

[16] Linares CF, Goldwasser MR, Machado FJ, Rivera A, Rodríguez-Fuentes G, Barrault J. Advantages of base exchanged natural clinoptilolite as a catalyst for the Knoevenagel reaction. Microporous and Mesoporous Materials. 2000;**41**:69-77. DOI: 10.1016/S1387-1811(00)00274-2

[17] Moreno-Tost R, Santamaría-González J, Rodríguez-Castellón E, Jiménez LA, Autié MA, González E, et al. Selective catalytic reduction of nitric oxide by ammonia over Cu-exchanged Cuban natural zeolites. Applied Catalysis B: Environmental. 2004;**50**:279-288. DOI: 10.1016/j.apcatb.2004.01.019

[18] Arcoya A, Seoane XL, Soria J. Effect of iron on the deactivation of Ni/clinoptilolite catalysts by thiophene poisoning. Journal of Chemical Technology and Biotechnology. 1997;**68**:171-176. DOI: 10.1002/(SICI)1097-4660(199702)68:2<171:AID-JCTB621>3.0.CO;2-D

[19] Lee HC, Woo HC, Chung SH, Kim HJ, Lee KH, Lee JS. Effects of metal cation on the skeletal isomerization of 1-butene over clinoptilolite. Journal of Catalysis. 2002;**211**:216-225. DOI: 10.1006/jcat.2002.3732

[20] Royaee SJ, Falamaki C, Sohrabi M, Ashraf Talesh SS. A new Langmuir-Hinshelwood mechanism for the methanol to dimethylether dehydration reaction over clinoptilolite-zeolite catalyst. Applied Catalysis A: General. 2008;**338**:114-120. DOI: 10.1016/j.apcata.2008.01.011

[21] Nimwattanakul W, Luengnaruemitchai A, Jitkarnka S. Potential of Ni supported on clinoptilolite catalysts for carbon dioxide reforming of methane. International Journal of Hydrogen Energy. 2006;**31**:93-100. DOI: 10.1016/j.ijhydene.2005.02.005

[22] Özçelik Z, Soylu GSP, Boz I. Catalytic combustion of toluene over Mn, Fe and Co-exchanged clinoptilolite support. Chemical Engineering Journal. 2009;**155**:94-100. DOI: 10.1016/j.cej.2009.07.013

[23] Huirache-Acuña R, Rivera-Muñoz EM, Pawelec B, Ostrooumov M, Maya-Yescas R, Rico JL. The use of a natural Mexican zeolite as support of NiMoW sulfide hydrotreating catalysts. Catalysis Today. 2014;**220-222**:301-309. DOI: 10.1016/j.cattod.2013.07.019

[24] Thommes M, Kaneko K, Neimark AV, Oliver JP, Rodriguez-Reinoso F, Rouquerol J, et al. Physisorption of gases, with special reference to the evaluation of surface area and pore size distribution (IUPAC technical report). Pure and Applied Chemistry. 2015;**87**(9-10):1051-1069. DOI: 10.1515/pac-2014-1117

[25] Groen JC, Peffer LAA, Moulijn JA, Pérez-Ramírez J. Mesoporosity development in ZSM-5 zeolite upon optimized desilication conditions in alkaline medium. Colloids and Surfaces A: Physicochemical and Engineering Aspects. 2004;**241**:53-58. DOI: 10.1016/jcolsurfa.2004.04.012

[26] Kruk M, Jaroniec M, Ko CH, Ryoo R. Characterization of the porous structure of SBA-15. Chemistry of Materials. 2000;**12**:1961-1968. DOI: 10.1021/cm000164e

[27] Lewandowski M, Sarbak Z. The effect of boron addition on hydrodesulfurization and hydrodenitrogenation activity of NiMo/Al_2O_3 catalysts. Fuel. 2000;**79**:487-495. DOI: 10.1016/S0016-2361(99)00151-9

[28] Olivas A, Zepeda TA. Impact of Al and Ti ions on the dispersion and performance of supported NiMo(W)/SBA-15 catalysts in the HDS and HYD reactions. Catalysis Today.

2009;**143**:120-125. DOI: 10.1016/j.cattod.2008.09.001

[29] Del Arco M, Carrazan SRG, Martin C, Martin I, Rives V. A FTIR assessment of surface acidity and dispersion of surface species in titania and alumina-supported molybdena. Spectrochimica Acta. 1994;**50**:697-702. DOI: 0584-8539/94

[30] Zink N, Annal TH, Pansiot J, Yella A, Banhart F, Tremel W. In situ heating TEM study of onion-like WS_2 and MoS_2 nanostructures obtained via MOCVD. Chemistry of Materials. 2008;**20**(1):65-71. DOI: 10.1021/cm061867k

[31] Gutierrez OY, Klimova T. Effect of the support on the high activity of the (Ni)Mo/ZrO_2-SBA-15 catalyst in the simultaneous hydrodesulfurization of DBT and 4,6-DMDBT. Journal of Catalysis. 2011;**281**:50-62. DOI: 10.1016/j.jcat.2011.04.001

[32] Thompson RK, Hilsenbeck SJ, Paskach TJ, McCarley RE, Schrader GL. Pretreatment of new reduced ternary molybdenum sulfide catalysts. Journal of Molecular Catalysis A: Chemical. 2000;**161**(1-2):75-87. DOI: 10.1016/S1381-1169(00)00143-6

[33] Finster J. SiO_2 in 6:3 (stishovite) and 4:2 Co-ordination-characterization by core level spectroscopy (XPS/XAES). Surface and Interface Analysis. 1988;**12**:309-314. DOI: 10.1002/sia.740120507

[34] Lee DK, Lee HT, Lee IC, Park SK, Bae SY, Kim CW, et al. W-incorporated CoMo/γ-Al_2O_3 hydrodesulfurization catalyst: II characterization. Journal of Catalysis. 1996;**159**:219-229. DOI: 10.1006/jcat.1996.9999

[35] Díaz de León JN, Zavala-Sánchez LA, Suárez-Toriello VA, Alonso-Núñez G, Zepeda TA, Yocupicio RI, et al. Support effect of NiW catalysts for highly selective sulfur removal from light hydrocarbons. Applied Catalysis B: Environmental. 2017;**213**:167-176. DOI: 10.1016/j.catb.2017.05.014

[36] Pawelec B, Navarro RM, Campos-Martin JM, López-Agudo A, Vasudevan PT, Fierro JLG. Silica–alumina-supported transition metal sulphide catalysts for deep hydrodesulphurization. Catalysis Today. 2003;**86**:73-85. DOI: 10.1016/S0920-5861(03)00405-X

[37] Venezia AM, Raimondi F, La Parola V, Deganello G. Influence of sodium on the structure and HDS activity of Co-Mo catalysts supported on silica and aluminosilicate. Journal of Catalysis. 2000;**194**:393-400. DOI: 10.1006/jcat.2000.2953

[38] Nikolova D, Edreva-Kardjieva R, Giurginca RM, Meghea A, Vakros J, Voyiatzis GA, et al. The effect of potassium addition on the state of the components in the oxide precursor of the (Ni)(Mo)/γ-Al_2O_3 water-gas shift catalysts: FT-IR, diffuse reflectance and Raman spectroscopic studies. Vibrational Spectroscopy. 2007;**44**:343-350. DOI: 10.1016/j.vibspec.2007.03.002

[39] Lindner J, Sachdev A, Schwank J, Villa-Garcia M. Characterization and hydrodesulfurization activity studies of unpromoted molybdenum sulfides prepared by elemental solid state reaction. Journal of Catalysis. 1992;**137**(2):333-345. DOI: 10.1016/0021-9517(92)90161-A